*Geotechnical Aspects of Underground Construction in Soft Ground – Negro & Cecilio Jr. (Eds)*
*© 2018 Taylor & Francis Group, London, ISBN 978-1-138-29711-1*

# The role of building position on the response of buildings to tunnelling subsidence: Numerical modelling

G. Giardina
*Department of Architecture and Civil Engineering, University of Bath, Bath, UK*

S. Ritter, M.J. DeJong & R.J. Mair
*Department of Engineering, University of Cambridge, Cambridge, UK*

ABSTRACT: The potential damage caused by tunnel excavations to surface buildings can be effectively investigated by centrifuge testing. However, for practical reasons only a limited number of geometrical configurations can be tested in a geotechnical centrifuge. Therefore, numerical modelling provides an essential tool to generalise the laboratory results.

This paper illustrates the performance of a 2D finite element model of masonry buildings subjected to tunnelling in sand. The results of the first series of centrifuge tests performed on complex 3D printed masonry structures and presented in the companionpaper were used for the model validation. The model includes nonlinear constitutive laws for both the soil and the building.

Differently than previous works, this paper focuses on the accurate simulation of the building response by using structural parameters specifically defined for the assessment of building deformations. The results provide insights into the effect of different building positions relative to the tunnel on the structural response. The validated model can be used to investigate the effect of different building conditions on the soil-structure interaction mechanism.

## 1 INTRODUCTION

The preliminary phase of every underground project in urban areas requires a robust assessment of the potential settlement-induced damage to surface structures. The accuracy of the assessment depends on the correct understanding of the complex interaction between the excavation process and the soil and building response.

While field observations from previous projects offer invaluable data to identify the nature and magnitude of the involved mechanisms (e.g. Burland et al. 2001), they give only limited information on specific cause-effect relationships, due to the concurrent presence of interacting effects. Laboratory tests performed on scaled models subjected to pre-defined settlements with controlled boundary conditions and continuous response monitoring have been used to quantify the relationships between the source and effect of ground settlements (Laefer et al. 2011), (Giardina et al. 2012), although the soil-structure interaction is not directly modelled. Centrifuge testing is particularly effective to reproduce the prototype conditions in a scaled model of a soil-structure interaction problem (Taylor and Grant 1998, Caporaletti et al. 2006, Farrell et al. 2014, Ritter et al. 2017).

However, the time and laboratory resources which are necessary to perform experiments in a geotechnical centrifuge enable the investigation of a limited number of selected case scenarios. Therefore, numerical modelling can be used to generalise experimental results. Among the available computational models of tunnelling-induced soil-structure interaction (Burd et al. 2000, Liu et al. 2000, Son and Cording 2005, Boonpichetvong and Rots 2005, Franzius et al. 2006, Giardina et al. 2010, Pickhaver et al. 2010, Giardina et al. 2013, Amorosi et al. 2014, Losacco et al. 2014), few have been validated against centrifuge results (e.g. Giardina et al. 2015) and none of those focused on the detailed assessment of the building response.

In this paper, the results of centrifuge tests performed on complex 3D printed structures of masonry buildings are used to validate a coupled soil-tunnel-building finite element model. The model is first evaluated through comparison of displacements at the soil surface and the base of the structure. Then structural parameters specifically selected to evaluate the building deformations are used to compare the numerical and experimental outcomes. These comparisons are conducted for a set of three centrifuge tests with the same structure located in different positions with respect

to the tunnel to evaluate the effect building position on the building deformation.

## 2 NUMERICAL MODEL

The 2D finite element model reproduced the 1:75 centrifuge scaled model of a 3D printed building subject to tunnelling in sand (Fig. 1). The soil was modelled by quadratic plane strain elements with a nonlinear elastic behaviour (Table 1):

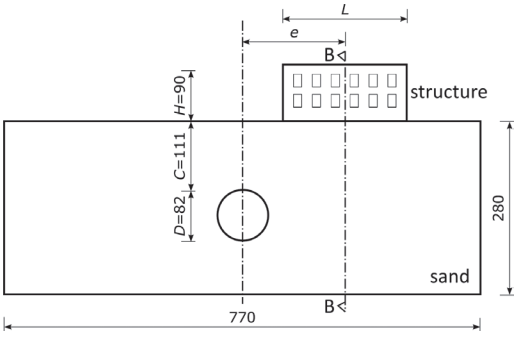


Figure 1. Geometry of the 2D numerical model reproducing the centrifuge setup.

Table 1. Material inputs for the numerical model.

| | | |
|---|---|---|
| Structure | Young's modulus | $E_w = 0.8 \times 10^3$ N/mm$^2$ |
| | Density | $\rho_w = 1.28 \times 10^{-6}$ kg/mm$^3$ |
| | Poisson's ratio | $\nu_w = 0.2$ |
| | Tensile strength | $f_{tw} = 1.27$ |
| | Ultimate strain | $\varepsilon_w = 0.31\%$ |
| Soil | Ref. Young's modul. | $E_0 = 25$ N/mm$^2$ |
| | Density | $\rho_m = 1.59 \times 10^{-6}$ kg/mm$^3$ |
| | Poisson's ratio | $\nu_m = 0.25$ |
| | Ref. shear modulus | $G_1 = 1$ N/mm$^2$ |
| | Ref. compr. modulus | $K_1 = 2.5$ N/mm$^2$ |
| | Power constant | $n = 0.53$ |
| | Ref. pressure | $p_0 = -1 \times 10^{-3}$ N/mm$^2$ |
| Interface | Normal stiffness | $k_n = 100$ N/mm$^3$ |
| | Tangent stiffness | $k_t = 1$ N/mm$^3$ |
| | Cohesion | $c = 0$ N/mm$^2$ |
| | Friction angle | $\phi = 30°$ |
| | Dilatancy angle | $\psi = 0°$ |

$$\begin{cases} \varepsilon_v = \dfrac{1}{K_1}\left(\dfrac{p}{p_0}\right)^{n-1}\left(1-\beta\dfrac{q^2}{p^2}\right)p \\ \varepsilon_s = \dfrac{1}{3G_1}\left(\dfrac{p}{p_0}\right)^{n-1} q \end{cases} \quad (1)$$

where $\varepsilon_v$ is the isotropic strain invariant, $\varepsilon_s$ is the shear strain invariant, $p$ is the total mean normal stress, $q$ is the deviatoric stress, $K_1$ is the reference compression modulus, $G_1$ is the reference shear modulus, $n$ is a constant coefficient, $p_0$ is the reference pressure, equal to –1 kPa, and $\beta = \frac{K_1(1-n)}{6G_1}$.

The soil parameters were calibrated by comparison with centrifuge spin-up displacements (Giardina et al. 2015). In the numerical simulation, first a 75 g acceleration was applied to the model, to reproduce the centrifuge conditions. Second, a radial pressure was applied to the tunnel boundary to reproduce the initial soil stresses. Finally, the tunnelling-induced settlement profile was obtained by progressively reducing this radial pressure.

The centrifuge 3D-printed structure was modelled by quadratic plane strain elements characterised by a smeared rotating crack model with elastic behaviour in compression and post-cracking linear softening in tension. In order to include the contribution of the transversal walls and footing foundation to the global building stiffness, the parameters of the 3D printed material (Table 1) were modified according to the out of plane geometry. Details about this procedure can be found in Giardina et al. (2016). The building was connected to the soil through line interface elements with zero tensile strength and frictional behaviour. The interface parameters were calibrated by comparison with the tunnelling-induced horizontal displacements of the soil surface which were observed in the experiment.

The numerical analyses presented in this paper correspond to the centrifuge tests illustrated in Figure 2. They explore the influence of the tunnelling-induced settlement profile on the structure; the shape of the profile depends on the position of the building with respect to the tunnel. With reference to the dimensions illustrated in Figure 1, three different values for the eccentricity $e$ were assumed; $e$ = 0, (sagging, Fig. 1a), $e$ = 160

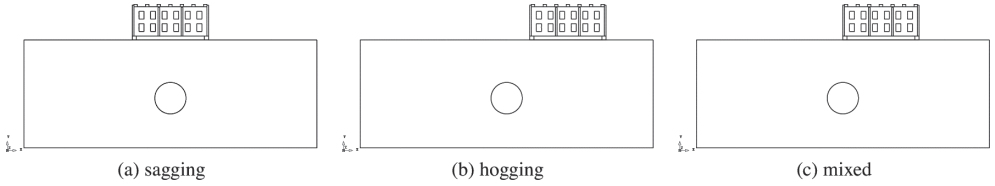


Figure 2. Numerical model: building position with respect to the tunnel.

(hogging, Fig. 2b) and $e = 100$ (mixed profile, with the greenfield inflection point contained within the building footprint, Fig. 2c). The model included strip footing foundations, four transversal walls and windows covering 20% of the façade area.

## 3 DEFORMATION PARAMETERS

Figure 3 illustrates the parameters used to quantify the building deformation (Son and Cording 2005).

Top horizontal strain:

$$\varepsilon_{h,\text{top}} = \frac{\Delta x_D - \Delta x_C}{L} \tag{2}$$

Base horizontal strain:

$$\varepsilon_{h,\text{base}} = \frac{\Delta x_A - \Delta x_B}{L} \tag{3}$$

Slope:

$$s = \frac{\Delta y_A - \Delta y_B}{L} \tag{4}$$

Tilt:

$$\theta = \frac{\Delta x_B - \Delta x_C}{H} \tag{5}$$

Angular distortion:

$$\beta = s - \theta \tag{6}$$

These parameters were evaluated for each bay of both the experimental and numerical models by using the reference points shown in Figure 4.

## 4 RESULTS

This section reports the validation of the numerical model in terms of displacements, interface stresses and deformation parameter values. An overview of the building deformed shapes for the three cases at volume loss $V_L = 4\%$ is given in Figure 5.

Figure 6 shows the vertical displacements of the soil surface for increasing volume losses. In the sagging case the model reproduced the embedment of the building corners into the soil (Fig. 6a); this phenomenon is combined with the development of a gap between the building base and the soil. The comparison between the soil (Fig. 6a) and building (Fig. 7a) displacements confirms the presence of the gap in both the experimental and numerical models: for increasing volume losses the soil displacements are progressively larger than the building base displacements. This phenomenon is also reflected by the distribution of the interface stresses (Figs. 8a,d), which progressively reduce in the middle of the structure and become zero at the moment of the gap formation, while they increase under the embedding corners. For realistic volume losses (up to 2%), both

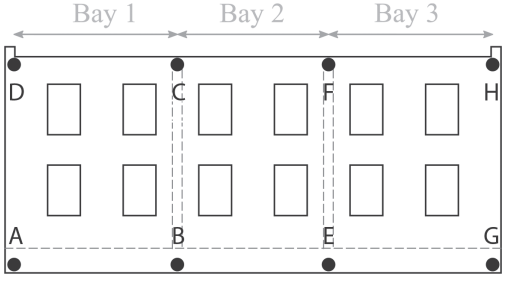


Figure 4. Building reference points and deformation parameters.

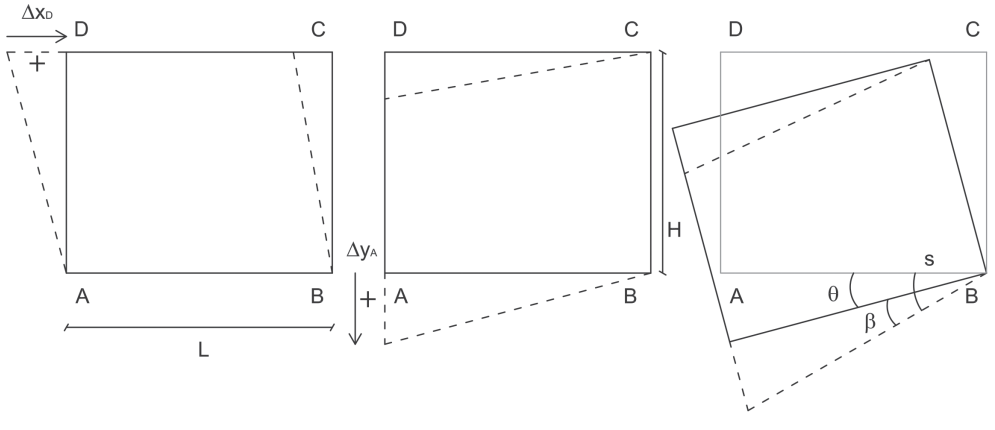


Figure 3. Deformation parameters used to compare the numerical and experimental deformation of each building bay.

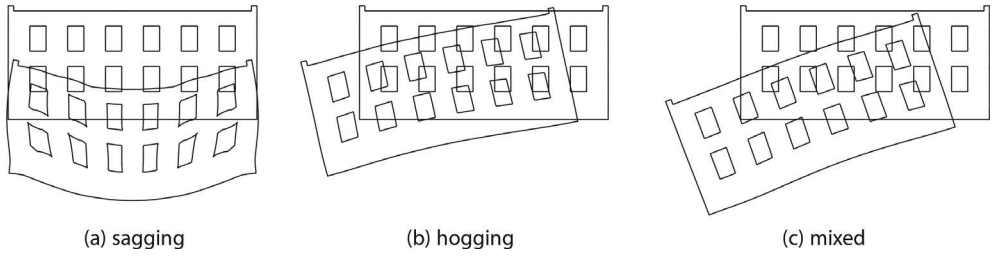


Figure 5. Tunnelling-induced building deformed shape, $V_L = 4\%$, magnification factor = 100.

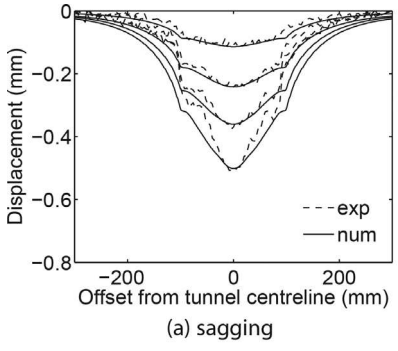


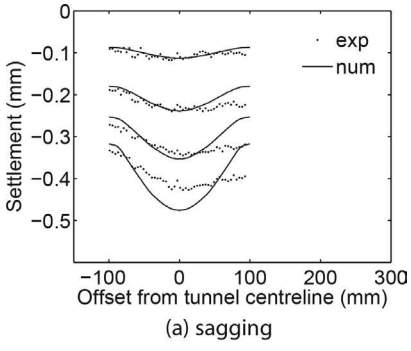


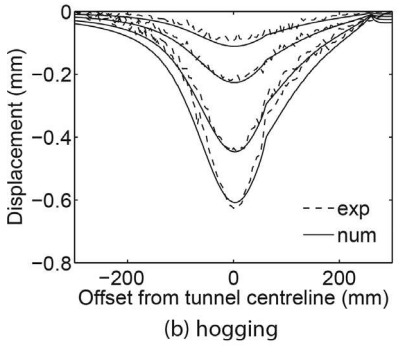


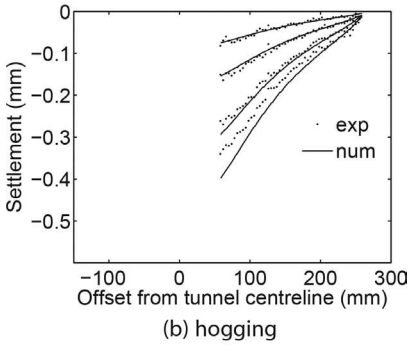


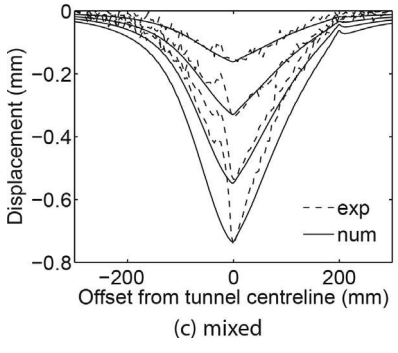


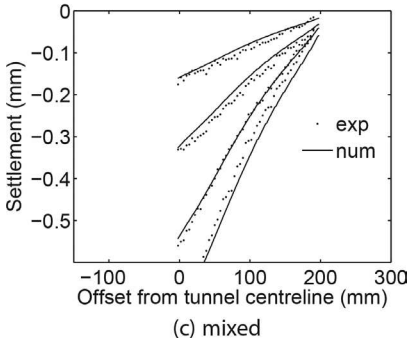


Figure 6. Vertical displacements of the soil surface during tunnelling at $V_L = 0.5,1,2$ and 4%.

Figure 7. Vertical displacements of the structure base during tunnelling at $V_L = 0.5,1,2$ and 4%.

the soil and building numerical curves match well the experimental results. A bigger discrepancy is observed at $V_L = 4\%$, mainly because the nonlinear elastic soil model cannot capture the failure chimney mechanism developing above the tunnel.

The numerical model also reproduced the settlement profile flattened by the building in the hogging position (Fig. 6b), as well as the increased displacement above the tunnel centreline at the building corner for the mixed case (Fig. 6c). Figs 7b and 7c confirm a good simulation of the building base displacements. Figures 8b,e and 8c,f show that for the hogging and mixed case the building foundation never loses contact with the soil; this is consistent with the experimental observations. A reduction in interface stresses with increasing volume loss is visible for the hogging case (Fig. 8e); for the mixed case, the increasing interface stresses at the left corner (Figs. 8c,f) are compatible with the larger displacements displayed in Figures 6c and 7c.

Before validation of the numerical model in terms of building deformation parameters, Figures 9 and 10 compares the experimental and numerical displacements of selected reference points (see Fig. 4). While the vertical displacements are reproduced correctly in both trend and magnitude, the numerical horizontal displacements for the hogging and mixed cases (Fig. 10b,c) are significantly larger than the experimental values.

Figures 11 to 19 compare the structural parameters defined in Section 3 for each bay of the experimental and numerical models. In this way, the numerical model is evaluated for the specific purpose of assessing the building deformations. The most significant parameters are the top and base horizontal strains, which give a direct indication of the building bending deformation, and the angular distortion, which provides a measure of the shear deformation.

In the sagging case (Figs. 11a, 12a and 13a) all bays exhibit a compressive top horizontal strain, which is consistent with the concave settlement profile induced by the volume loss. Both the sign and the magnitude of the numerical strains match

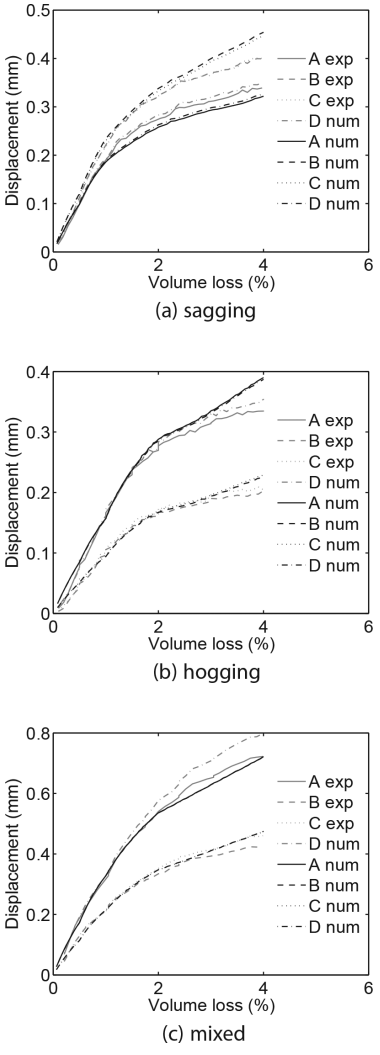


Figure 9. Vertical displacements of bay 1 reference points, comparison between experimental and numerical model.

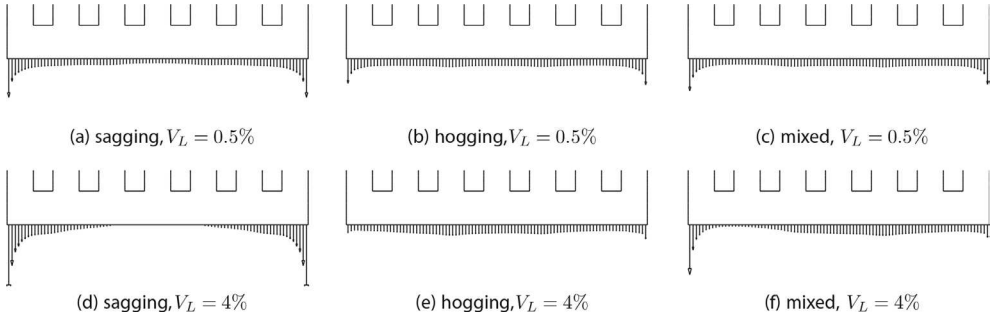


Figure 8. Vector plot of base interface stresses at $V_L = 4\%$.

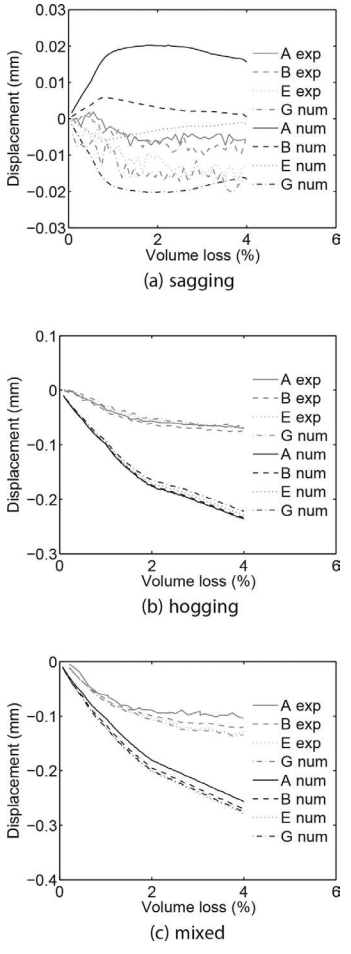


Figure 10. Horizontal displacements of base reference points, comparison between experimental and numerical model.

the experimental observations well. The numerical model predicts base horizontal strains similar to the top ones, while the centrifuge tests show almost negligible strains at the base, as an effect of the rough soil-structure interaction (Figs. 11b, 12b and 13b). The shear deformation assessment tends to be conservative, with angular distortions slightly larger than the experimental results.

In the hogging case, the numerically predicted top horizontal strains are negative for all bays, consistently with the overall building deformation (Figs. 14a, 15a and 16a). Thepredicted strains are relatively accurate, with the exception of bay 1, where the centrifuge test resulted in negligible top strains. The base horizontal strains show the same tendency of being underestimated, though not uniformly (Figs. 14b, 15b and 16b). The predicted angular distortion curves are also relatively accurate (Figs. 14e, 15e and 16e), noting the minimal angular distortion that occurred in bay 2.

The numerical model provides a good simulation of the centrifuge testing also for both the bending and shear deformation indicators of the structure spanning the sagging and hogging zone (Figs. 17, 18 and 19). Ê The main difference is observed in the simulation of the top horizontal strains of the part of the building closest to the tunnel centreline (Fig. 17a) and the base horizontal strains of the opposite building side (Fig. 19b). The numerical model shows negligible top horizontal tensile strains in bay 1, where the experimental model exhibits compressive behaviour; similarly, it shows a small tensile deformation at the base in bay 3, where the experimental model is again in compression. Conversely, the numerical model simulates well the increasing tensile strains for increasing volume losses at the top of bay 2 (Fig. 18a) and the corresponding increasing compressive base strains (Fig. 18b).

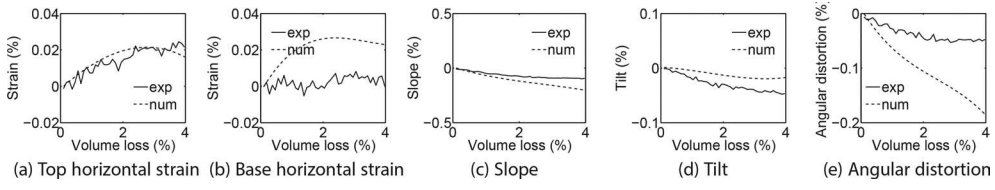


Figure 11. Structure response parameters, sagging case, bay 1.

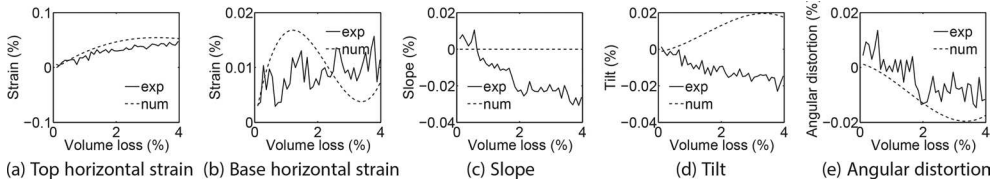


Figure 12. Structure response parameters, sagging case, bay 2.

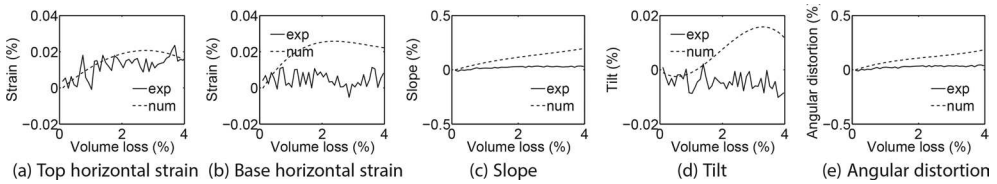


Figure 13. Structure response parameters, sagging case, bay 3.

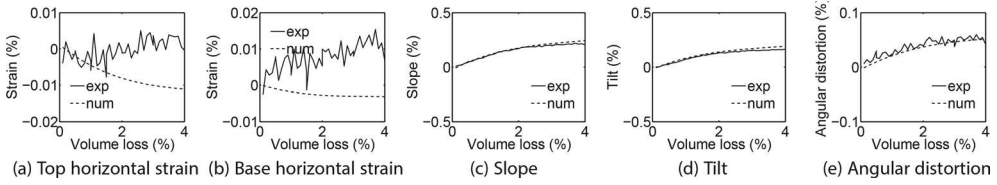


Figure 14. Structure response parameters, hogging case, bay 1.

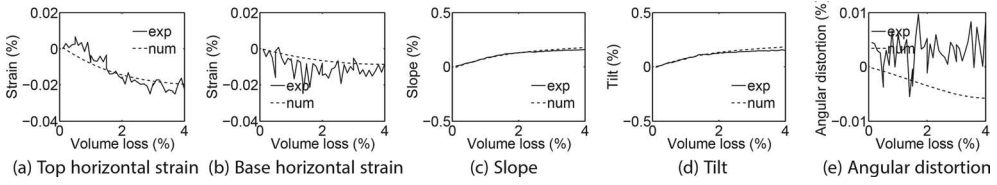


Figure 15. Structure response parameters, hogging case, bay 2.

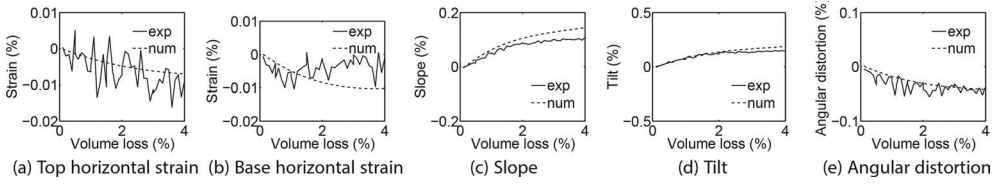


Figure 16. Structure response parameters, hogging case, bay 3.

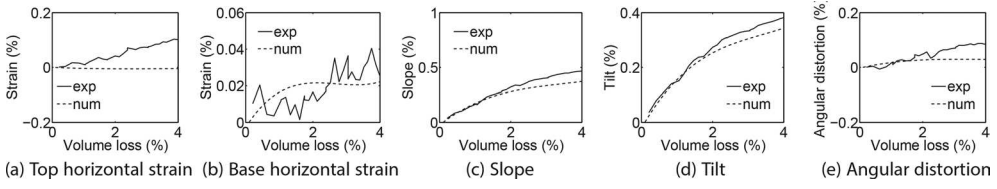


Figure 17. Structure response parameters, mixed case, bay 1.

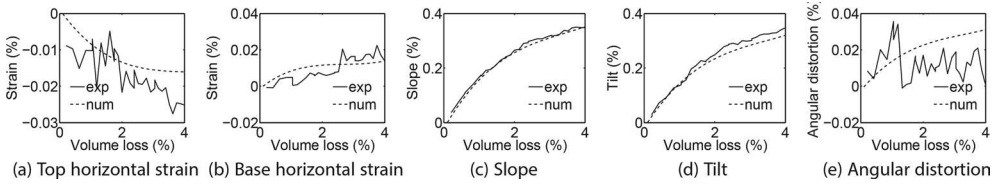


Figure 18. Structure response parameters, mixed case, bay 2.

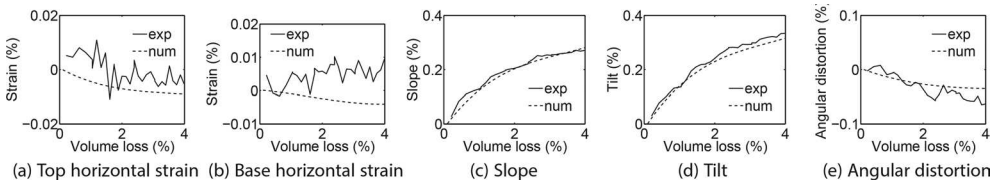


Figure 19. Structure response parameters, mixed case, bay 3.

## 5 CONCLUSIONS

This paper presented the validation of a 2D finite element model aiming at predicting the structural response of masonry structures adjacent to tunnel excavations. The coupled behaviour of the soil, the tunnel and the building have been compared with the results of centrifuge testing including complex 3D-printed building models. The performance of the model has been assessed against structural parameters quantifying the local deformations of building units. The numerical results showed a good agreement with the experimentally observed indicators of rigid body rotation and bending and shear deformations. The model has the potential to be used in more extensive studies of material and geometrical factors governing the interaction between tunnelling, soil subsidence and building damage.

## ACKNOWLEDGMENTS

The authors are grateful to EPSRC grant EP/KP018221/1 and Crossrail for providing financial support. The related research data is available at https://doi.org/10.17863/CAM.6836.

## REFERENCES

Amorosi, A., D. Boldini, G. De Felice, M. Malena, & M. Sebastianelli (2014). Tunnelling-induced deformation and damage on historical masonry structures. *Geotechnique 64*(2), 118–130.

Boonpichetvong, M. & J.G. Rots (2005). Settlement damage of masonry buildings in soft-ground tunnelling. *Structural Engineer 83*(1), 32–37.

Burd, H.J., G.T. Houlsby, C.E. Augarde, & L. G (2000). Modelling tunnelling-induced settlement of masonry buildings. *Proc Inst Civil Eng: Geotech Eng 143*(1), 17–29.

Burland, J., J. Standing, & F. Jardine (2001). *Building response to tunnelling: case studies from construction of the Jubilee Line Extension, London.* CIRIA Special Publication Series. London: Thomas Telford.

Caporaletti, P., A. Burghignoli, & R.N. Taylor (2006). Centrifuge study of tunnel movements and their interaction with structures. In Bakker (Ed.), *Geotechnical Aspects of Underground Construction in Soft Ground,* London. Taylor & Francis.

Farrell, R., R. Mair, A. Sciotti, & A. Pigorini (2014). Building response to tunnelling. *Soils and Foundations 54*(3), 269–279.

Franzius, J.N., D.M. Potts, & J.B. Burland (2006). The response of surface structures to tunnel construction. *Proc Inst Civil Eng: Geotech Eng 159*(1), 3–17.

Giardina, G., M. DeJong, & R. Mair (2015). Interaction between surface structures and tunnelling in sand: Centrifuge and computational modelling. *Tunnelling and Underground Space Technology 50,* 465–478.

Giardina, G., A. v. d. Graaf, M.A.N. Hendriks, J.G. Rots, & A. Marini (2013). Numerical analysis of a masonry fac¸ade subject to tunnelling-induced settlement. *Engineering Structures 54,* 234–247.

Giardina, G., M.A.N. Hendriks, & J.G. Rots (2010). Numerical analysis of tunnelling effects on masonry buildings: the influence of tunnel location on damage assessment. *Advanced Materials Research 133,* 289–294.

Giardina, G., A. Marini, M.A.N. Hendriks, J.G. Rots, F. Rizzardini, & E. Giuriani (2012). Experimental analysis of a masonry fac¸ade subject to tunnelling-induced settlement. *Engineering Structures 45,* 421–434.

Giardina, G., S. Ritter, M. DeJong, & R. Mair (2016, September). Modelling the 3D brittle response of masonry buildings to tunnelling. In *10th International Conference in Structural Analysis of Historical Constructions,* Leuven.

Laefer, D.F., L.T. Hong, A. Erkal, J.H. Long, & E.J. Cording (2011). Manufacturing, assembly, and testing of scaled, historic masonry for one-gravity, pseudo-static, soil-structure experiments. *Construction and Building Materials 25*(12), 4362–4373.

Liu, G., G.T. Houlsby, & C.E. Augarde (2000). 2-dimensional analysis of settlement damage to masonry buildings caused by tunnelling. *Structural Engineer 79*(1), 19–25.

Losacco, N., A. Burghignoli, & L. Callisto (2014). Uncoupled evaluation of the structural damage induced by tunnelling. *Géotechnique 64,* 646–656(10).

Pickhaver, J.A., H.J. Burd, & G.T. Houlsby (2010, October). An equivalent beam method to model masonry buildings in 3D finite element analysis. *Computers & Structures 88*(19–20), 1049–1063.

Ritter, S., G. Giardina, M. DeJong, & M.R.J. (2017). Centrifuge modelling of building response to tunnel excavation. *Journal of Physical Modelling in Geotechnics.* (Accepted for publication).

Son, M. & E. Cording (2005). Estimation of building damage due to excavation-induced ground movements. *Journal of Geotechnical and Geoenvironmental Engineering 131*(2), 162–177.

Taylor, R. & R. Grant (1998). Centrifuge modelling of the influence of surface structures on tunnelling induced ground movements. In J.N. Ferreira (Ed.), *Tunnels and Metropolises,* Rotterdam, pp. 261–265. Balkema.